

Chiral state transfer under dephasingKonghao Sun  and Wei Yi*

CAS Key Laboratory of Quantum Information, University of Science and Technology of China, Hefei 230026, China;
CAS Center For Excellence in Quantum Information and Quantum Physics, Hefei 230026, China;
and Hefei National Laboratory, University of Science and Technology of China, Hefei 230088, China



(Received 2 January 2023; accepted 20 June 2023; published 5 July 2023)

Exceptional points emerge in the complex eigenspectra of non-Hermitian systems, and give rise to rich critical behaviors. An outstanding example is the chiral state transfer, where states can swap under an adiabatic encircling around the exceptional point, but only along one direction. In dissipative quantum systems, such exceptional-point encirclings are often accompanied by decoherence, whose impact is beyond the description of non-Hermitian Hamiltonians. In this paper, we study in detail the effects of dephasing on the encircling dynamics, adopting the full Lindblad master equation. Introducing experimentally relevant quantum-jump processes that account for dephasing, we show that gaps emerge in the eigenspectra landscape of the corresponding Liouvillian superoperator. It follows that the chiral state transfer does not take place in the adiabatic limit, since the system always adiabatically follows the quasisteady state of the Liouvillian regardless of the encircling direction. Nevertheless, the chirality is restored at intermediate encircling times, where the dynamics is nonadiabatic in both encircling directions, distinct from the typical chiral state transfer in non-Hermitian systems. While our results are applicable to several recent experiments, we examine a recent cold-atom experiment in particular, and show that the observed long-time chirality is limited to the special encircling path therein. Our paper provides further insight into the chiral state transfer under experimental conditions, and is helpful for controlling open-system dynamics from the perspective of non-Hermitian physics.

DOI: [10.1103/PhysRevA.108.013302](https://doi.org/10.1103/PhysRevA.108.013302)**I. INTRODUCTION**

An open quantum system exchanges energy, particle, or information with its environment, and thus defies the description of Hermitian Hamiltonians. A convenient, if phenomenological, alternative is provided by the non-Hermitian framework [1]. With complex eigenspectra and ramified symmetries [2], non-Hermitian Hamiltonians exhibit rich and exotic features, including the parity-time symmetry [3–14], the non-Hermitian nodal phases [15–19], and non-Hermitian topology [20–34]. These phenomena have stimulated intense research interest in recent years, not only because of the fresh insights they offer regarding open systems, but also for their potential applications.

The recent surge of interest in non-Hermitian physics can be traced back to the discovery of the parity-time symmetry [3,4], under which a non-Hermitian Hamiltonian can acquire a completely real eigenspectrum. At the critical point where the symmetry becomes spontaneously broken, eigenenergies and eigenstates coalesce, as the eigenspectrum transits from being completely real to complex. These so-called exceptional points (EPs), while absent in Hermitian systems, generally exist in non-Hermitian settings, even without the parity-time symmetry [35]. Their sensitive dependence on the tuning parameters and spectral landscapes is promising for enhanced sensing [36–38] and quantum-device design [39–41]. In the

latter case, a particularly useful feature is the chiral state transfer near an EP [42–47]. By slowly varying the parameters on a closed loop near the EP (encircling the EP is preferred but not necessary), the dynamics could lead to a state exchange, depending on the direction of the encircling—the state is switched only one way around. Though seemingly contradictory to the adiabatic theorem, the chiral state transfer is a consequence of the complex eigenspectral structure in the parameter space, together with the path-dependent amplification of the nonadiabatic couplings [46].

Experimentally, the chiral state transfer has been observed in classical systems with gain and loss [48,49], and in dissipative quantum settings of photons [50], superconducting qubits [51,52], trapped ions [53], solid spins [54], and cold atoms [55]. In quantum systems, the non-Hermiticity can be realized by enforcing postselection [56,57]. More specifically, most of these open quantum systems feature weak interactions with a Markovian environment, with the full, unconditional dynamics described by a Lindblad master equation. The time evolution of the Lindblad master equation can be understood as the average of infinitely many quantum trajectories, each represented by a stochastic wave function, whose time evolution is driven by a non-Hermitian effective Hamiltonian and interrupted by quantum jumps. Hence, for trajectories where quantum jumps are absent, their quantum-state dynamics are driven by the non-Hermitian effective Hamiltonian. Enforcing postselection constitutes picking out these trajectories, along which the dynamics are governed by the non-Hermitian effective Hamiltonian alone. This is called conditional dynamics,

*wyiz@ustc.edu.cn

as the dynamics are conditioned upon the absence of quantum jumps [1]. However, realistic open systems often consist of many degrees of freedom, wherein additional quantum-jump processes are inevitable. In a series of recent experiments [51,52,55], for instance, it has been demonstrated that the EP-induced chiral state transfer persists despite these additional quantum jumps. This is perhaps not too surprising, if the quantum-jump processes are to be glossed as perturbations whose impact on the non-Hermitian dynamics manifests only as decoherence or heating. But from the perspective of open quantum systems, it is more appropriate to analyze the dynamics using the full Lindblad master equation, where the time evolution of the density matrix is driven by the Liouvillian superoperator. Since the Liouvillian is intrinsically non-Hermitian and can host its own EPs [51,52,58,59], it is natural to pose the question whether the impact of the quantum jumps on the EP-induced chiral state exchange can be understood from the Liouvillian spectra. The question is nontrivial, not least because the spectral landscape of Liouvillians, along with the Liouvillian EPs, are in general distinct from those of the corresponding non-Hermitian Hamiltonians. Dynamics can therefore be quite different when the decoherence-inducing quantum jumps are present.

In this paper, we focus on the chiral state transfer under quantum-jump processes that lead to dephasing. These terms are relevant in recent experiments of EP encirclings in superconducting qubits [51,52] and cold atoms [55]. We start from the full Lindblad master equation, and demonstrate that the presence of quantum-jump processes opens up a finite gap in the eigenspectra landscape of the Liouvillian. A direct consequence is that the chiral state transfer does not occur when the encircling time approaches infinity. When the encircling time is long enough, the system always ends up in a quasisteady state of the Liouvillian, regardless of the encircling direction. While the chirality of the state transfer can be restored at intermediate encircling times, the dynamics then is distinct from that under the non-Hermitian Hamiltonian. In the non-Hermitian case, the encircling dynamics is adiabatic in one direction and nonadiabatic in the other, and the final state is a pure state. By contrast, under dephasing and at intermediate times, the dynamics in either direction is nonadiabatic, and the final state is mixed. We note that our analysis does not rely on the connection between EPs of the non-Hermitian Hamiltonian and the Liouvillian EPs, and is therefore distinct from previous theoretical studies of hybrid Liouvillian setups [58,59].

In the light of these understandings, we discuss the recent EP-encircling experiment in cold atoms [55]. Therein, non-Hermiticity is implemented by postselecting the internal states of atoms undergoing laser-induced spontaneous decay. However, branching of the spontaneous decay necessarily gives rise to additional quantum-jump processes, causing dephasing and heating. While the experiment reports chiral state transfer under a fairly long encircling time, we show that this is facilitated by the particular choice of the encircling path in the experiment. Therein, the path consists of a segment where the dynamics is driven by a purely Hermitian Hamiltonian. The Liouvillian gap closes along this segment, such that the dynamics is decidedly nonadiabatic on the Liouvillian eigenspectral landscape in either encircling direction. We

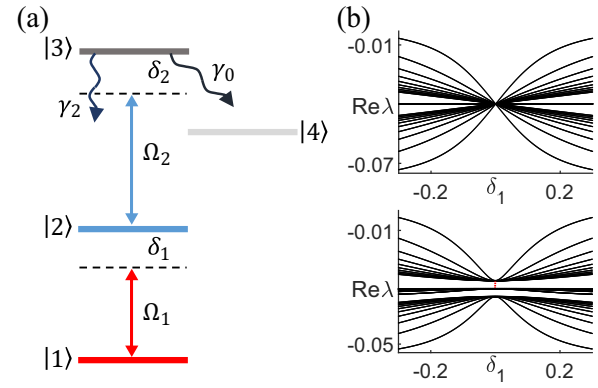


FIG. 1. (a) Schematic illustration of the four-level system considered in this paper. States $|1\rangle$ and $|2\rangle$ are coupled with a coupling rate Ω_1 and detuning δ_1 . Dissipation is introduced by coupling states $|2\rangle$ and $|3\rangle$ with a rate Ω_2 and detuning δ_2 . The spontaneous decay rates for $|3\rangle \rightarrow |4\rangle$ and $|3\rangle \rightarrow |2\rangle$ are denoted, respectively, as γ_0 and γ_2 . (b) The real components of the Liouvillian spectra $\text{Re}\lambda$ without (upper panel) and with (lower panel) the recycling term $L_\phi \rho L_\phi^\dagger$, respectively (see the main text for the definition of L_ϕ). A Liouvillian gap is opened in the lower panel, as indicated by the vertical dashed line in the lower panel. The parameters in (b) are $\gamma_0 = 50$, $\Omega_2 = 1$, $\delta_2 = 0$, and $\Omega_1 = 0.1, 0.2, 0.3, 0.4, 0.5, 0.6, 0.7, 0.8, 0.9, 1$. We take $\gamma_2 = 0$ ($\gamma_2 = 10$) for the upper (lower) panel. Here Ω_2 is taken as the unit of energy.

demonstrate that, by choosing a more general encircling path, the chiral state transfer occurs only at intermediate encircling times, consistent with our prediction above. The effect of the Liouvillian-gap closing along the Hermitian segment can therefore be understood as pushing the chirality condition from the intermediate-time to the infinite-time limit.

Our paper is organized as follows. In Sec. II, we present the four-level system that we consider, inspired by the recent cold-atom experiment. We analyze the encircling dynamics in detail in Sec. III. In Sec. IV, we discuss the experiment [55] from the perspective of the Liouvillian eigenspectrum, and consider a general encircling path where the results in Sec. III can be recovered. We conclude in Sec. V.

II. MODEL

Motivated by the recent experiments [51,52,55], we consider a four-level system illustrated in Fig. 1. The two-level open system is encoded in the states $\{|1\rangle, |2\rangle\}$, which are coupled to each other. For simplicity, we assume the coupling does not involve momentum transfer, so that the external degrees of freedom are decoupled. A laser-induced loss is imposed on state $|2\rangle$ by coupling it to an excited state $|3\rangle$, which undergoes spontaneous decay. We consider the case where the decay has two different channels, one into a bystander state $|4\rangle$, the other back into state $|2\rangle$. Adiabatically eliminating state $|3\rangle$ and projecting out state $|4\rangle$, we derive the Lindblad master equation governing the dynamics of the open system (see the Appendix for a detailed derivation where we

take $\hbar = 1$):

$$\dot{\rho} = -i(H_{\text{eff}}\rho - \rho H_{\text{eff}}^\dagger) + L_\phi \rho L_\phi^\dagger - \frac{1}{2}L_\phi^\dagger L_\phi \rho - \frac{1}{2}\rho L_\phi^\dagger L_\phi, \quad (1)$$

where the non-Hermitian effective Hamiltonian is

$$H_{\text{eff}} = H_0 - i\Gamma|2\rangle\langle 2|. \quad (2)$$

In the basis of $\{|1\rangle, |2\rangle\}$, the matrix for the Hermitian part of the Hamiltonian is

$$H_0 = \begin{bmatrix} \frac{\delta_1}{2} & -\Omega_1 \\ -\Omega_1^* & -\frac{\delta_1}{2} \end{bmatrix}, \quad (3)$$

where the coupling rate Ω_1 and the detuning δ_1 are illustrated in Fig. 1. The quantum-jump operator $L_\phi = \sqrt{\gamma_\phi}|2\rangle\langle 2|$ accounts for the spontaneous decay $|3\rangle \rightarrow |2\rangle$, which leads to the dephasing of the $\{|1\rangle, |2\rangle\}$ subsystem. The non-Hermitian term in Eq. (2) characterized by Γ originates from the decay $|3\rangle \rightarrow |4\rangle$, and is enforced through postselection in the experiment by considering dynamics of atoms in the states $|1\rangle$ and $|2\rangle$ only [55,60]. Explicit expressions for γ_ϕ and Γ in terms of the control parameters $\Omega_{1,2}$, $\delta_{1,2}$, and $\gamma_{0,2}$ (all illustrated in Fig. 1) are summarized in the Appendix.

In the absence of the decay process $|3\rangle \rightarrow |2\rangle$, the dynamics of the subsystem $\{|1\rangle, |2\rangle\}$ is driven by the non-Hermitian effective Hamiltonian H_{eff} . It is based on similar non-Hermitian Hamiltonians with which EP encircling and chiral state transfer were studied in recent experiments [55]. The decay channel $|3\rangle \rightarrow |2\rangle$, besides modifying Γ and introducing an additional non-Hermitian contribution $\frac{1}{2}L_\phi^\dagger L_\phi$ to H_{eff} , gives rises to the quantum recycling term $L_\phi \rho L_\phi^\dagger$ that is responsible for dephasing (see the Appendix).

The impact of dephasing is further visible on the eigenspectral landscape of the Liouvillian superoperator \mathcal{L} . Specifically, vectorizing the density matrix [58,61]

$$\rho = \begin{bmatrix} \rho_{11} & \rho_{12} \\ \rho_{21} & \rho_{22} \end{bmatrix} \rightarrow |\psi\rangle = \begin{pmatrix} \rho_{11} \\ \rho_{12} \\ \rho_{21} \\ \rho_{22} \end{pmatrix}, \quad (4)$$

we cast the Liouvillian in the matrix form

$$\mathcal{L}_M = \begin{bmatrix} 0 & -i\Omega_1^* & i\Omega_1 & 0 \\ -i\Omega_1 & -i\delta_1 - \frac{|\Omega_2|^2\gamma^3}{\Delta^4} & 0 & i\Omega_1 \\ i\Omega_1^* & 0 & i\delta_1 - \frac{|\Omega_2|^2\gamma^3}{\Delta^4} & -i\Omega_1^* \\ 0 & i\Omega_1^* & -i\Omega_1 & -\frac{|\Omega_2|^2\gamma_0\gamma^2}{\Delta^4} \end{bmatrix}. \quad (5)$$

The density-matrix dynamics is then captured by $|\dot{\psi}\rangle = \mathcal{L}_M|\psi\rangle$ in an enlarged Hilbert space. The eigenspectrum λ of \mathcal{L} is defined as $\mathcal{L}_M|\phi\rangle = \lambda|\phi\rangle$. In Fig. 1(b), we show the real component of the Liouvillian spectrum $\text{Re}\lambda$ in the parameter space of (Ω_1, δ_1) , which has a significant impact on the system dynamics.

To see this, we define the right and left eigenvectors of \mathcal{L}_M as $\mathcal{L}_M|\phi_n^R\rangle = \lambda_n|\phi_n^R\rangle$ and $\langle\phi_n^L|\mathcal{L}_M = \langle\phi_n^L|\lambda_n$, where λ_n is the n th eigenvalue. We then express the density-matrix

dynamics as

$$|\Psi(t)\rangle = \sum_n e^{\text{Re}\lambda_n t + i\text{Im}\lambda_n t} \langle\phi_n^L|\Psi(0)\rangle|\phi_n^R\rangle. \quad (6)$$

While $\text{Re}\lambda_n \leq 0$ for dissipative systems, states with the smallest $|\text{Re}\lambda_n|$ are either steady states ($\text{Re}\lambda = 0$) or quasisteady states ($\text{Re}\lambda < 0$), toward which the dynamics would inevitably converge at long times according to Eq. (6).

In our system, the dynamics is not trace preserving, because of the population of state $|4\rangle$ which is outside of the two-level open system. This is manifested in the Liouvillian spectra as the deviation of the high-lying band from $\text{Re}\lambda = 0$. We therefore regard the high-lying band in Fig. 1(b) as the quasisteady state. Furthermore, the speed at which the quasisteady states are approached is determined by the Liouvillian gap, herein defined as the minimum spectral difference between the real eigenvalue of the quasisteady state and those of the other eigenstates of \mathcal{L} . According to Eq. (6), a finite Liouvillian gap indicates that the quasisteady state is approached exponentially fast. In our system, a Liouvillian gap emerges as soon as the recycling term is switched on [see Fig. 1(b)]. It follows that, under a slow parameter change (compared to the corresponding time scale of the Liouvillian gap), the system should adiabatically follow the quasisteady state, meaning the absence of the chiral state transfer.

III. EP ENCIRCLING UNDER DEPHASING

In the absence of dephasing ($\gamma_2 = 0$), an EP exists at $\{\delta_1 = 0, \Gamma = 2|\Omega_1|\}$ under H_{eff} alone. When the system parameters are adiabatically tuned in a closed loop near the EP, depending on the encircling direction, the time-evolved state can be switched or remain unchanged, on returning to the initial parameters. This is illustrated in Figs. 2(a) and 2(b) by the cyan trajectories, calculated according to

$$\bar{E}_0(t) = \frac{\sum_{i=\pm} |\langle\chi_i^L(t)|\psi_0(t)\rangle|^2 E_i(t)}{\sum_{i=\pm} |\langle\chi_i^L(t)|\psi_0(t)\rangle|^2}, \quad (7)$$

where $\langle\chi_i^L|$ ($i = \pm$) are left eigenstates of H_{eff} , with $H_{\text{eff}}^\dagger|\chi_i^L\rangle = E_i^*|\chi_i^L\rangle$, and E_\pm are the eigenvalues of H_{eff} . The time-evolved state $|\psi_0(t)\rangle$ is given by

$$i\frac{d}{dt}|\psi_0(t)\rangle = H_{\text{eff}}(t)|\psi_0(t)\rangle. \quad (8)$$

Such a chiral state transfer originates from the interplay of the topology of the eigenspectra landscape of the Hamiltonian in the parameter space, and the non-Hermitian amplification of the nonadiabatic coupling terms. As analyzed in previous theoretical studies and confirmed in various experiments, the dynamics adiabatically follows the eigenspectral landscape (the state gets switched) in one direction, and is nonadiabatic in the other (the state remains the same). Here the chirality is signaled by the different final states for different encircling directions. However, this is no longer the case when $\gamma_2 \neq 0$.

In the upper panels of Figs. 2(a) and 2(b), we show, respectively, the trajectories (in black) for the clockwise and counterclockwise encirclings in the presence of dephasing. We evolve the density matrix according to Eq. (1), and calculate the trajectories on the eigenspectra landscape E_\pm . Note

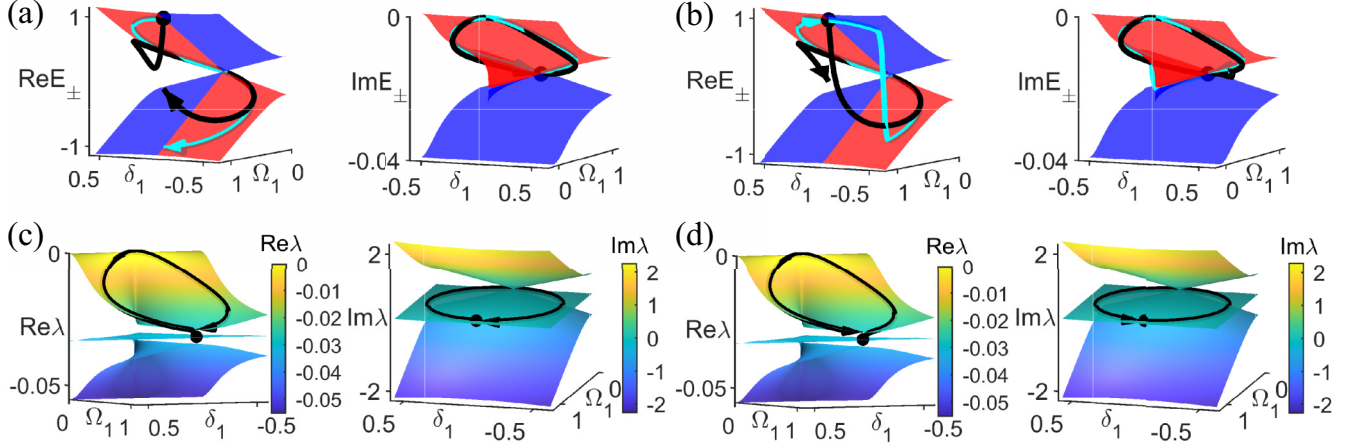


FIG. 2. Trajectories of the encircling dynamics in the adiabatic limit, for (a), (c) clockwise rotations and (b), (d) counterclockwise rotations. (a), (b) Trajectories (black and cyan) against the eigenspectra of the non-Hermitian Hamiltonian H_{eff} . The red (blue) color code indicates the eigenstate with a larger (smaller) imaginary component, and hence smaller (larger) loss. The black trajectory corresponds to the dynamics under the master equation, calculated using Eq. (9). The cyan trajectory corresponds to the ideal EP-encircling dynamics under H_{eff} alone, calculated using Eq. (7). (c), (d) Trajectories against the eigenspectra of the Liouvillian \mathcal{L} . The black trajectory is calculated according to Eq. (10). For all cases, the initial state is an eigenstate of H_{eff} , and the encircling path is $\delta_1(t) = 0.5 \sin(\pm 2\pi t/T)$ and $\Omega_1(t) = 0.5 + 0.5 \cos(\pm 2\pi t/T)$, with the total encircling time $T = 15000$. Other parameters are $\Omega_2 = 1$, $\gamma_0 = 50$, $\gamma_2 = 10$, and $\delta_2 = 0$. The units of energy and time are taken as Ω_2 and $1/\Omega_2$, respectively.

that, throughout our paper, we calculate the eigenspectra of H_{eff} by setting $\gamma_2 = 0$. Specifically, the trajectories in black are calculated according to

$$\bar{E}(t) = \frac{\sum_{i=\pm} \langle \chi_i^L(t) | \rho(t) | \chi_i^L(t) \rangle E_i(t)}{\sum_{i=\pm} \langle \chi_i^L(t) | \rho(t) | \chi_i^L(t) \rangle}. \quad (9)$$

The key observation from Figs. 2(a) and 2(b) is that, when the recycling term (or dephasing) is switched on, the chirality disappears—the final states of different encircling directions lie close together, and would asymptotically approach one another in the long-encircling-time limit (not shown here but see Fig. 4).

Such a behavior can be straightforwardly understood from the trajectories on the eigenspectra landscape of the Liouvillian. This is shown in Figs. 2(c) and 2(d), where the trajectories (in black) are calculated according to

$$\bar{\lambda}(t) = \frac{\sum_{i=1}^4 |\langle \phi_i^L(t) | \psi(t) \rangle|^2 \lambda_i(t)}{\sum_{i=1}^4 |\langle \phi_i^L(t) | \psi(t) \rangle|^2}, \quad (10)$$

where $|\psi(t)\rangle$ is the vectorized density matrix $\rho(t)$, and $|\phi_i^L(t)\rangle$ satisfies $\mathcal{L}_M^\dagger(t) |\phi_i^L(t)\rangle = \lambda_i^* |\phi_i^L(t)\rangle$. Apparently, because of the presence of the dephasing-induced Liouvillian gap, the state first relaxes to and then adiabatically follows the quasisteady state of the Liouvillian (high-lying band). The chirality thus vanishes.

However, when the total encircling time T is finite, the chiral behavior can emerge even under dephasing, though the dynamics is always nonadiabatic regardless of the encircling direction. This is illustrated in Fig. 3, where we choose an intermediate encircling time. Notice how the trajectories always involve nonadiabatic jumps, whether projected onto the spectral landscape of H_{eff} [as in Figs. 3(a) and 3(b)], or that of the Liouvillian \mathcal{L} [as in Figs. 3(c) and 3(d)]. This scenario

is actually what has been observed in [51,52], as we have numerically checked that the reported chiral state transfer would disappear at longer encircling times.

To quantify our observations above, we adopt the definition of chirality [52]

$$C = \frac{1}{2} \text{Tr}[\sqrt{(\tilde{\rho}_{\text{cw}} - \tilde{\rho}_{\text{ccw}})^\dagger (\tilde{\rho}_{\text{cw}} - \tilde{\rho}_{\text{ccw}})}]. \quad (11)$$

Here $\tilde{\rho}_{\text{cw,ccw}} = \rho_{\text{cw,ccw}} / \text{Tr}(\rho_{\text{cw,ccw}})$, with $\rho_{\text{cw,ccw}}$ being the final-time density matrix of the clockwise (cw) and counterclockwise (ccw) encircling. The chirality C takes values in between 0 and 1, and represents the distinguishability between the final density matrices for clockwise and counterclockwise encirclings. We have $C = 0$ when the two density matrices are the same, and $C = 1$ when they are orthogonal pure states.

We show the calculated chirality as a function of the encircling time T , for different γ_2 in Fig. 4(a). In the absence of dephasing ($\gamma_2 = 0$), C approaches a finite value close to unity in the long-time limit. By contrast, as long as γ_2 is finite, C always approaches zero for a sufficiently long encircling time. Another prominent feature of Fig. 4(a) is the emergence of a chirality peak at intermediate T , which corresponds to the parameter regime of the chiral transfer illustrated in Fig. 3. We note that the fast oscillatory behavior at small T [see inset of Fig. 4(a)] originates from the phase factor $e^{i\text{Im}\lambda_n t}$ in Eq. (6). Interestingly, the final-time chirality manifests a universal scaling with γ_2 and T , as shown in Fig. 4(b), with the relation $C = f(\gamma_2 T^{1/\nu})$. We have numerically checked that, while the scaling function $f(x)$ is trajectory dependent, ν appears to be universal and remains close to $\nu \approx 1.561$ regardless of the encircling path.

Hence, along a general encircling path, the chiral state transfer only emerges at intermediate encircling times under dephasing, which is qualitatively different from the EP-encircling dynamics in a purely non-Hermitian system. In

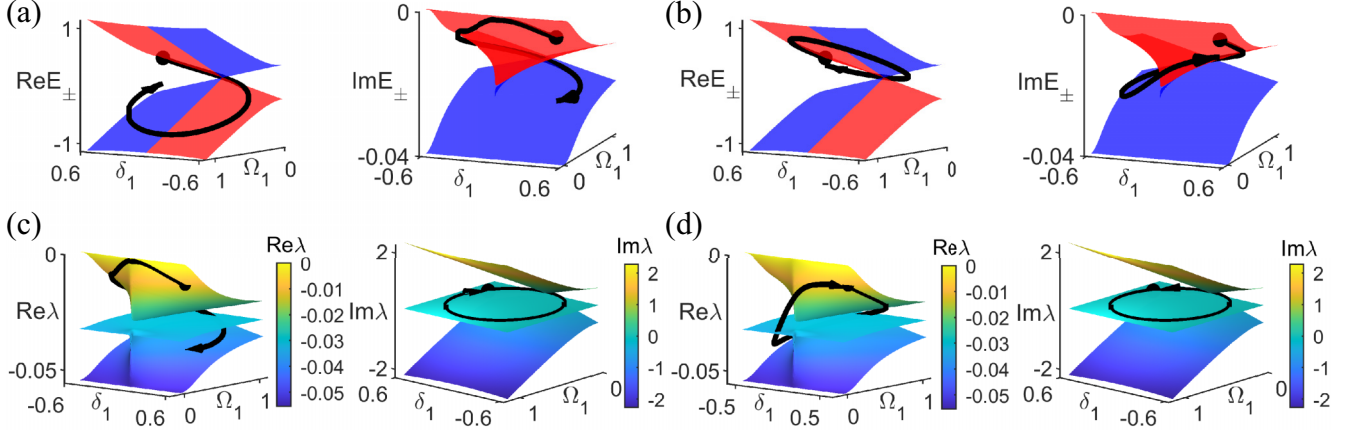


FIG. 3. Trajectories of the encircling dynamics for an intermediate encircling time $T = 150$, for (a), (c) clockwise rotations and (b), (d) counterclockwise rotations. (a), (b) Trajectories against the eigenspectra of the non-Hermitian Hamiltonian H_{eff} , calculated according to Eq. (9). (c), (d) Trajectories against the eigenspectra of the Liouvillian \mathcal{L} , calculated according to Eq. (10). The encircling path is $\delta_1(t) = 0.5 \sin(\pm 2\pi t/T + 2\pi/3)$ and $\Omega_1(t) = 0.5 + 0.5 \cos(\pm 2\pi t/T + 2\pi/3)$. Other parameters are the same as those in Fig. 2. The units of energy and time are taken as Ω_2 and $1/\Omega_2$, respectively.

the long-time limit, dephasing opens up a Liouvillian gap, and the dynamics is essentially adiabatic on the Liouvillian spectral landscape, regardless of the encircling direction. The conclusions above should apply to a series of recent experiments [51,52,55], where EP encircling has been studied in the presence of dephasing. Using numerical simulations, we have

checked that the chiral behavior reported in [51,52] indeed occurs only at intermediate encircling times, and disappears in the long-time limit. Nevertheless, such a conclusion seems to contradict the observations of a recent cold-atom experiment [55], where the chiral state transfer is observed at sufficiently long encircling time. In the following, we show that such an observation is based on the special encircling path adopted therein.

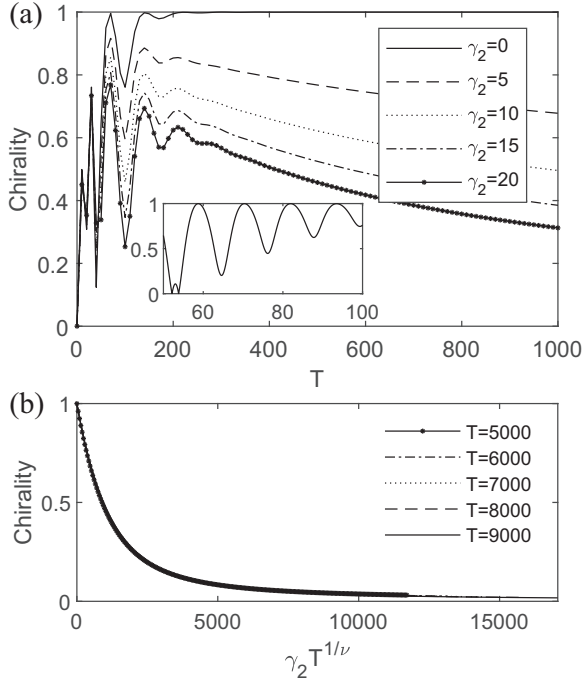


FIG. 4. (a) Chirality as a function of the total encircling time T under different values of γ_2 . The inset shows detailed oscillatory behavior of chirality for $\gamma_2 = 0$ where more data points are sampled within the range $T \in [50, 100]$. (b) Scaling relation of the chirality with respect to γ_2 and T . The initial state is $\rho(0) = |1\rangle\langle 1|$. We determine $\nu \approx 1.561$ from numerical fitting (see main text). The units of energy and time are taken as Ω_2 and $1/\Omega_2$, respectively.

IV. EXPERIMENTAL RELEVANCE

In [55], the collective chiral state transfer of an ultra-cold gas of fermions is observed, where the fermionic atoms are subject to a synthetic spin-orbit coupling and laser-induced atom loss. For atoms that remain in the system, their dynamics is driven by a non-Hermitian effective Hamiltonian with an EP embedded in the parameter space. The laser-induced loss, however, is accompanied by spontaneous decay back into the system, similar to the $|3\rangle \rightarrow |2\rangle$ decay channel in Fig. 1. Such a decay channel inevitably introduces decoherence to the system, which, according to our analysis above, should significantly impact the encircling dynamics.

To understand the experimental observation from the perspective of the master equation (1), we replace H_0 in Eq. (1) as

$$H_0 = \begin{bmatrix} \frac{\delta_1}{2} - 2q_x & -\Omega_1 \\ -\Omega_1^* & -\frac{\delta_1}{2} + 2q_x \end{bmatrix}, \quad (12)$$

which corresponds to the Hermitian part of the Hamiltonian in [55], within the momentum sector q_x (the q_x^2 terms are dropped since they are the same for the two spin components). For our calculations, we take the recoil energy $E_r = 2\pi \times 1.41$ kHz as the unit of energy, $k_r = \sqrt{2mE_r}$ (m is the atomic mass) as the unit of momentum, and $t_r = 1/E_r$ as the unit of time. We focus on the momentum sector $q_x/k_r = -0.81$, as the location of the Fermi surface under typical experimental conditions [55]. Taking typical experimental

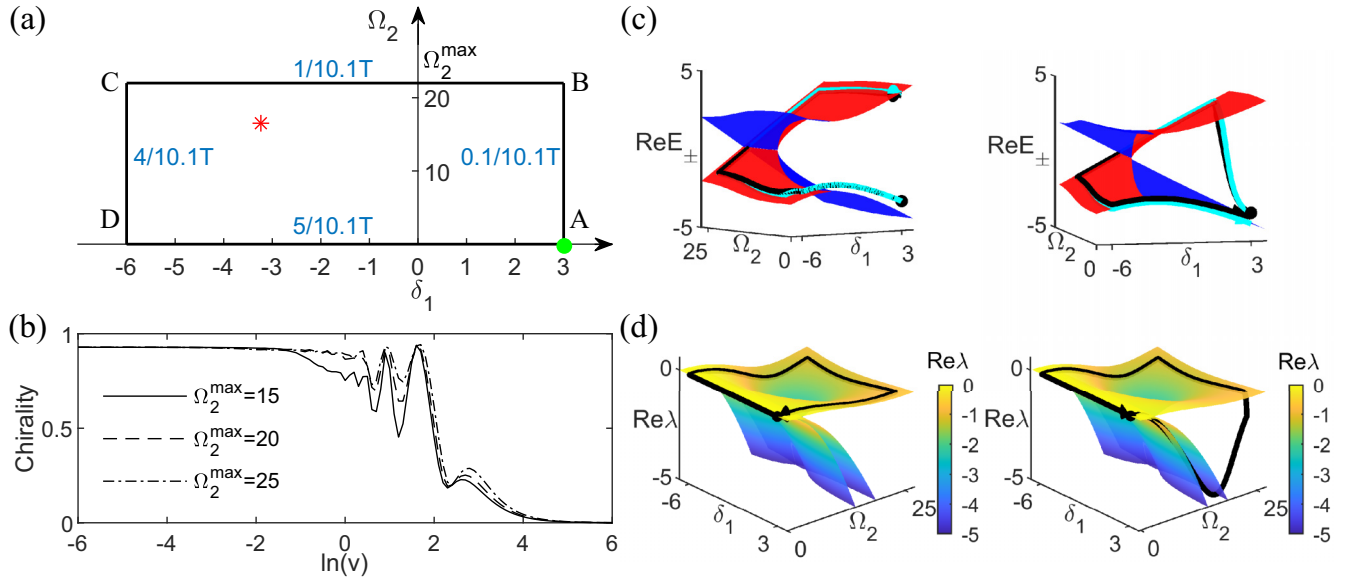


FIG. 5. (a) Encircling path adopted in the experiment [55]. For the various symbols, we adopt the convention in [55]: red star, the EP of H_{eff} in the parameter space; green dot, the initial point of encircling; blue numbers, the ratio of time spent on each segment. (b) Chirality as a function of $\ln(v)$ for various Ω_2^{max} . Here Ω_2^{max} is the maximum Ω_2 on the encircling path. (c), (d) Trajectories against the real eigenspectra of the non-Hermitian Hamiltonian H_{eff} (c) and the Liouvillian \mathcal{L} (d) for clockwise rotations (left panel) and counterclockwise rotations (right panel) for $\ln(v) = -2.66$. In (c), the black and cyan trajectories are calculated according to Eqs. (9) and (7), respectively. In (d), the black trajectory is calculated according to Eq. (10). Here the units of energy and time are respectively taken as the recoil energy $E_r = 2\pi \times 1.41$ kHz and $t_r = 1/E_r$.

parameters, we also fix $\gamma_0/E_r = 110.57$, $\gamma_2/E_r = 18.43$, $\Omega_1/E_r = -2.25$, and $\delta_2 = 0$ for our simulations below.

The experimental encircling path is reproduced in Fig. 5(a) and the calculated chiralities under different encircling times are plotted in Fig. 5(b). The initial parameters and state are, respectively, $\{\Omega_2/E_r = 3, \delta_1/E_r = 0\}$ (point A) and $\rho(0) = |2\rangle\langle 2|$. For the counterclockwise encircling, we first ramp up Ω_2 to Ω_2^{max} within the time $0.1/10.1T$ ($A \rightarrow B$), and then decrease δ_1/E_r to -6 within $1/10.1T$ ($B \rightarrow C$). This is followed by decreasing Ω_2/E_r to zero within $4/10.1T$ ($C \rightarrow D$), and ramping up δ_1/E_r to 3 ($D \rightarrow A$). The clockwise encircling ($A \rightarrow D \rightarrow C \rightarrow B \rightarrow A$) is the exact reverse process of the above. Since all the parameters are tuned in a linear fashion, we parametrize the encircling time by the encircling velocity $v = 2\pi/(T/t_r)$. The long-time limit is thus toward the left of the plot in Fig. 5(b), when v approaches zero. While the chirality peaks at intermediate velocities (or intermediate encircling times), it approaches unity when v approaches zero (or long encircling time). In [55], $\ln(v) \approx -2.66$, where the chirality is already approaching unity, as shown in Fig. 5(b). Under the same parameters, ideal EP encircling dynamics can be observed on the spectral landscape of the non-Hermitian Hamiltonian, as illustrated in Fig. 5(c). Curiously, this observation seems to contradict our conclusions in the previous section.

However, we notice that along the path AD in Fig. 5(a), $\Omega_2 = 0$ and the system is purely Hermitian. The Liouvillian gap closes along this sector. This renders our previous discussion irrelevant, as the open-system dynamics is typically nonadiabatic on the eigenspectral landscape of the Liouvillian. This is confirmed in Fig. 5(d). In the long-time limit, dynamics along BC and AD are both adiabatic: the system

follows the quasisteady state of the Liouvillian along BC , while it follows the eigenstate of the Hermitian Hamiltonian along AD . Along the segments AB and CD however, the dynamics can be nonadiabatic near the points D and A , respectively, because of the closing of the Liouvillian gap.

Upon closer examination, the observed chirality originates from the distinct eigenstate overlaps between those of the Hermitian Hamiltonian and the Liouvillian near the gap-closing points A and D . For the convenience of discussion, we denote the two eigenstates of the Hermitian Hamiltonian as $|\psi_{\pm}\rangle$, where $|\psi_+\rangle$ ($|\psi_-\rangle$) has a larger (smaller) eigenvalue. The system is initialized in the state $|2\rangle$ at point A , which is close (on the spectral landscape) to $|\psi_-\rangle$. For a counterclockwise rotation ($A \rightarrow B \rightarrow C \rightarrow D \rightarrow A$) starting in the state $\rho(0) = |2\rangle\langle 2|$ at point A , the density matrix is in the quasisteady state of the Liouvillian when approaching the gap-closing point D . Since the local quasisteady state has a large overlap with $|\psi_-\rangle$ near point D , the system is projected onto a mixed state with considerable overlap with $|\psi_-\rangle$ upon the gap closing. Following the adiabatic evolution along DA , the final state is then a mixed state that is close to $|\psi_-\rangle$ at point A , and is also close to the initial state. By contrast, for a clockwise rotation ($A \rightarrow D \rightarrow C \rightarrow B \rightarrow A$), the quasisteady state is projected onto a mixed state that is close to $|\psi_+\rangle$ near point A along BA . The final state is therefore nearly orthogonal to the initial state.

We then adopt a different, and more general, encircling path, as shown in Fig. 6. As expected, the chirality drops to zero again in the long-time limit. This leaves an intermediate encircling time as the only window to observe the chiral state transfer in the presence of decoherence.

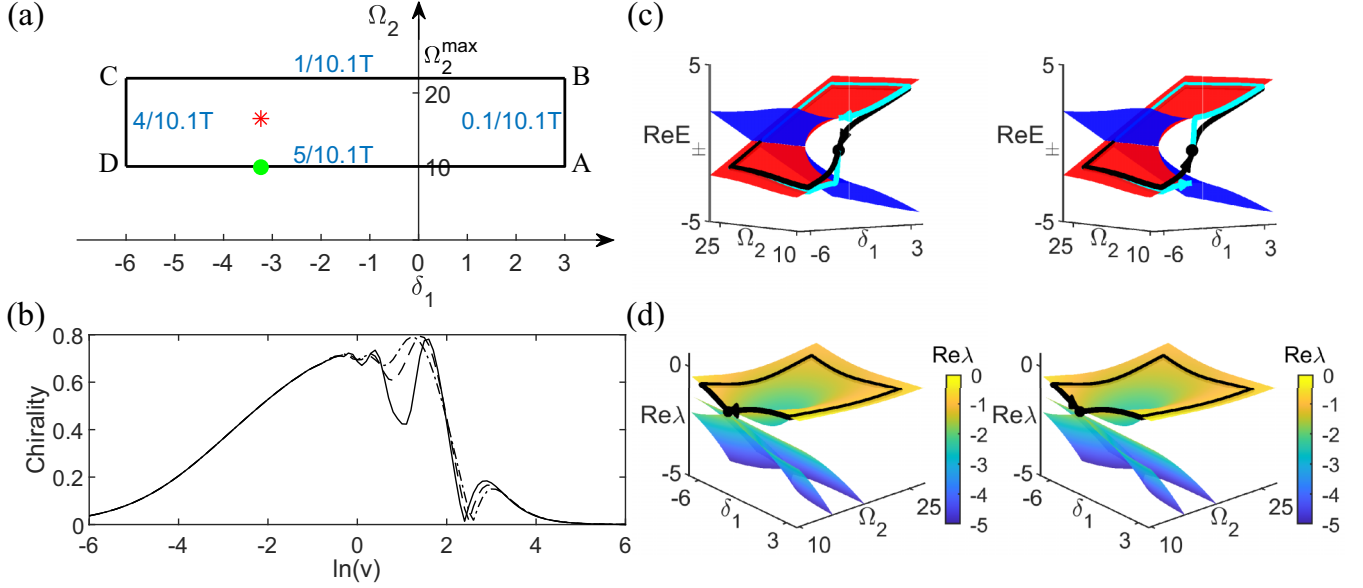


FIG. 6. (a) A more general encircling path, with no purely Hermitian segments. (b) Chirality as a function of $\ln(v)$ for various Ω_2^{\max} . As in Fig. 5(b), the solid line represents $\Omega_2^{\max} = 15$, the dashed line represents $\Omega_2^{\max} = 20$, and the dash-dot line represents $\Omega_2^{\max} = 25$. Other parameters are the same as those in Fig. 5. (c), (d) Trajectories against the real eigenspectra of the non-Hermitian Hamiltonian H_{eff} (c) and the Liouvillian \mathcal{L} (d) for clockwise rotations (left panel) and counterclockwise rotations (right panel) when $\ln(v) = -6$. Calculations of the trajectories are the same as those in Fig. 5. The units of energy and time are respectively taken as the recoil energy $E_r = 2\pi \times 1.41$ kHz and $t_r = 1/E_r$.

V. CONCLUSION

We study the impact of dephasing on the chiral state transfer near EPs in quantum open systems. We show that quantum jumps responsible for dephasing open up a Liouvillian gap, making the dynamics in the long-time limit necessarily adiabatic. Chiral state transfer thus typically emerges at intermediate times as an intrinsically nonadiabatic process. We discuss recent experiments in the light of our results. Specifically, in [51,52], the observed chiral transfer in the superconducting qubits belongs to the nonadiabatic category, which would disappear under a longer encircling time. On the other hand, the cold-atom experiment [55] observes chiral transfer at long times thanks to the special path therein where the Liouvillian gap closes.

Throughout our paper, we consider only the intrinsic dynamics, assuming a decoupling between the external (momentum) and internal degrees of freedom. For an atomic gas with lossy spin-orbit coupling as in [55], the recoil momentum accompanying the dephasing (quantum jump) process should also be considered for a better description of the system, particularly in regards to heating. We leave these considerations to future studies. Our results provide a unified understanding for EP encirclings in quantum open systems, and are of direct relevance to ongoing experimental efforts and quantum device design under realistic conditions.

ACKNOWLEDGMENTS

We thank Gyu-Boong Jo for helpful communications. This work has been supported by the National Natural Science

Foundation of China (Grant No. 11974331) and the Innovation Program for Quantum Science and Technology (Grant No. 2021ZD0301200).

APPENDIX: DERIVATION OF EQ. (1)

Dynamics of the system illustrated in Fig. 1 is governed by the Lindblad master equation

$$\dot{\rho} = -i[H, \rho] + \sum_{i=0,1} \left[L_i \rho L_i^\dagger - \frac{1}{2} \{L_i^\dagger L_i, \rho\} \right], \quad (\text{A1})$$

where $L_0 = \sqrt{\gamma_0}|4\rangle\langle 3|$ and $L_1 = \sqrt{\gamma_2}|2\rangle\langle 3|$. In the rotating frame, with the rotating wave approximation the equations of matrix elements are

$$\begin{aligned} \dot{\rho}_{11} &= i\Omega_1\rho_{21} - i\rho_{12}\Omega_1^* \\ \dot{\rho}_{12} &= -i[\rho_{13}\Omega_2^* + \delta_1\rho_{12} + \Omega_1(\rho_{11} - \rho_{22})] \\ \dot{\rho}_{13} &= -\rho_{13}(\gamma + i\delta_1 + i\delta_2) - i\Omega_2\rho_{12} + i\Omega_1\rho_{23} \\ \dot{\rho}_{21} &= i[\rho_{31}\Omega_2 + \delta_1\rho_{21} + \Omega_1^*(\rho_{11} - \rho_{22})] \\ \dot{\rho}_{22} &= \gamma_2\rho_{33} + i[\rho_{12}\Omega_1^* - \rho_{23}\Omega_2^* - \Omega_1\rho_{21} + \Omega_2\rho_{32}] \\ \dot{\rho}_{23} &= i[\rho_{23}(\gamma + i\delta_2) + \rho_{13}\Omega_1^* + \Omega_2(\rho_{33} - \rho_{22})] \\ \dot{\rho}_{31} &= -\rho_{31}(\gamma - i\delta_1 - i\delta_2) + i\Omega_2^*\rho_{21} - i\Omega_1^*\rho_{32} \\ \dot{\rho}_{32} &= -i[-i\rho_{32}(\gamma - i\delta_2) + \rho_{31}\Omega_1 + \Omega_2^*(\rho_{33} - \rho_{22})] \\ \dot{\rho}_{33} &= i(2i\gamma\rho_{33} + \rho_{23}\Omega_2^* - \Omega_2\rho_{32}) \end{aligned} \quad (\text{A2})$$

with $\gamma = (\gamma_0 + \gamma_2)/2$. The dynamics involving the state $|4\rangle$ is decoupled from that in the subspace of $\{|1\rangle, |2\rangle, |3\rangle\}$.

Assuming $\gamma \gg |\Omega_{1,2}|$, we set $\dot{\rho}_{13} = 0$, $\dot{\rho}_{23} = 0$, $\dot{\rho}_{33} = 0$, $\dot{\rho}_{31} = 0$, and $\dot{\rho}_{32} = 0$. We then have

$$\begin{aligned}
\dot{\rho}_{11} &= -i\rho_{12}\Omega_1^* + i\Omega_1\rho_{21} \\
\dot{\rho}_{12} &= -i\rho_{12} \left\{ \delta_1 - \frac{i|\Omega_2|^2 \{2\gamma(\gamma - i\delta_1 - i\delta_2)(|\Omega_2|^2 + \gamma^2 + \delta_2^2) + |\Omega_1|^2[|\Omega_2|^2 + 2\gamma(\gamma + i\delta_2)]\}}{2\gamma\Delta^4} \right\} \\
&\quad + i\Omega_1\rho_{22} \left\{ 1 - \frac{|\Omega_2|^2[|\Omega_1|^2 + (\gamma - i\delta_2)(\gamma - i\delta_1 - i\delta_2)]}{\Delta^4} \right\} + \frac{\Omega_1^2|\Omega_2|^4}{2\gamma\Delta^4}\rho_{21} - i\Omega_1\rho_{11} \\
\dot{\rho}_{21} &= i\rho_{21} \left\{ \delta_1 + \frac{i|\Omega_2|^2 \{2\gamma(\gamma + i\delta_1 + i\delta_2)(|\Omega_2|^2 + \gamma^2 + \delta_2^2) + |\Omega_1|^2[|\Omega_2|^2 + 2\gamma(\gamma - i\delta_2)]\}}{2\gamma\Delta^4} \right\} \\
&\quad - i\Omega_1^*\rho_{22} \left\{ 1 - \frac{|\Omega_2|^2[|\Omega_1|^2 + (\gamma + i\delta_2)(\gamma + i\delta_1 + i\delta_2)]}{\Delta^4} \right\} + \frac{|\Omega_2|^4(\Omega_1^*)^2}{2\gamma\Delta^4}\rho_{12} + i\rho_{11}\Omega_1^* \\
\dot{\rho}_{22} &= -\frac{\gamma_0\rho_{22}|\Omega_2|^2[|\Omega_1|^2 + \gamma^2 + (\delta_1 + \delta_2)^2]}{\Delta^4} + i\Omega_1\rho_{21} \left\{ -1 + \frac{(2\gamma - \gamma_2)|\Omega_2|^2[|\Omega_1|^2 + (\gamma + i\delta_2)(\gamma + i\delta_1 + i\delta_2)]}{2\gamma\Delta^4} \right\} \\
&\quad - i\rho_{12}\Omega_1^* \left\{ -1 + \frac{(2\gamma - \gamma_2)|\Omega_2|^2[|\Omega_1|^2 + (\gamma - i\delta_2)(\gamma - i\delta_1 - i\delta_2)]}{2\gamma\Delta^4} \right\}
\end{aligned} \tag{A3}$$

where

$$\Delta^4 = |\Omega_1|^2[|\Omega_2|^2 + 2\gamma^2 - 2\delta_2(\delta_1 + \delta_2)] + [\gamma^2 + (\delta_1 + \delta_2)^2](|\Omega_2|^2 + \gamma^2 + \delta_2^2) + |\Omega_1|^4. \tag{A4}$$

Since $\Delta^4 \sim \gamma^4$, we keep terms at least of the order of γ^{-1} in Eq. (A3) to get

$$\dot{\rho} = -i \begin{bmatrix} -\Omega_1\rho_{21} + \rho_{12}\Omega_1^* & (\delta_1 - \frac{i\gamma^3|\Omega_2|^2}{\Delta^4})\rho_{12} + \Omega_1(\rho_{11} - \rho_{22}) \\ -\Omega_1^*(\rho_{11} - \rho_{22}) - (\delta_1 + \frac{i\gamma^3|\Omega_2|^2}{\Delta^4})\rho_{21} & -\frac{i\gamma_0\gamma^2\rho_{22}^2}{\Delta^4} - \rho_{12}\Omega_1^* + \Omega_1\rho_{21} \end{bmatrix}. \tag{A5}$$

This equation can be expressed as

$$\dot{\rho} = -i(H_{\text{eff}}\rho - \rho H_{\text{eff}}^\dagger) + L_\phi\rho L_\phi^\dagger - \frac{1}{2}L_\phi^\dagger L_\phi\rho - \frac{1}{2}\rho L_\phi^\dagger L_\phi, \tag{A6}$$

with $L_\phi = \sqrt{\gamma_\phi}|2\rangle\langle 2|$, $\gamma_\phi = \frac{\gamma_0\gamma^2|\Omega_2|^2}{\Delta^4}$, and

$$H_{\text{eff}} = \begin{bmatrix} \frac{\delta_1}{2} & -\Omega_1 \\ -\Omega_1^* & -\frac{\delta_1}{2} - \frac{i\gamma_0\gamma^2|\Omega_2|^2}{2\Delta^4} \end{bmatrix} = H_0 - i\Gamma|2\rangle\langle 2|, \tag{A7}$$

where $\Gamma = \frac{\gamma_0\gamma^2|\Omega_2|^2}{2\Delta^4}$. This gives us Eq. (1) in the main text.

-
- [1] Y. Ashida, Z. Gong, and M. Ueda, *Adv. Phys.* **69**, 249 (2020).
[2] K. Kawabata, K. Shiozaki, M. Ueda, and M. Sato, *Phys. Rev. X* **9**, 041015 (2019).
[3] C. M. Bender and S. Boettcher, *Phys. Rev. Lett.* **80**, 5243 (1998).
[4] C. M. Bender, S. Boettcher, and P. N. Meisinger, *J. Math. Phys.* **40**, 2201 (1999).
[5] C. E. Rüter, K. G. Makris, R. El-Ganainy, D. N. Christodoulides, M. Segev, and D. Kip, *Nat. Phys.* **6**, 192 (2010).
[6] J. Schindler, A. Li, M.-C. Zheng, F. M. Ellis, and T. Kottos, *Phys. Rev. A* **84**, 040101(R) (2011).
[7] S. Bittner, B. Dietz, U. Günther, H. L. Harney, M. Miski-Oglu, A. Richter, and F. Schäfer, *Phys. Rev. Lett.* **108**, 024101 (2012).
[8] C. Hang, G.-X. Huang, and V. V. Konotop, *Phys. Rev. Lett.* **110**, 083604 (2013).
[9] H. Jing, Ş. K. Özdemir, X.-Y. Lü, J. Zhang, L. Yang, and F. Nori, *Phys. Rev. Lett.* **113**, 053604 (2014).
[10] B. Peng, Ş. K. Özdemir, F.-C. Lei, F. Monifi, M. Gianfreda, G.-L. Long, S.-H. Fan, F. Nori, C. M. Bender, and L. Yang, *Nat. Phys.* **10**, 394 (2014).
[11] R. Fleury, D. Sounas, and A. Alù, *Nat. Commun.* **6**, 5905 (2015).
[12] Z.-Y. Zhang, Y.-Q. Zhang, J.-T. Sheng, L. Yang, M.-A. Miri, D. N. Christodoulides, B. He, Y.-P. Zhang, and M. Xiao, *Phys. Rev. Lett.* **117**, 123601 (2016).
[13] P. Peng, W.-X. Cao, C. Shen, W.-Z. Qu, J.-M. Wen, L. Jiang, and Y.-H. Xiao, *Nat. Phys.* **12**, 1139 (2016).
[14] L. Feng, R. El-Ganainy, and L. Ge, *Nat. Photon.* **11**, 752 (2017).
[15] Y. Xu, S.-T. Wang, and L.-M. Duan, *Phys. Rev. Lett.* **118**, 045701 (2017).
[16] J. C. Budich, J. Carlström, F. K. Kunst, and E. J. Bergholtz, *Phys. Rev. B* **99**, 041406(R) (2019).
[17] J. Carlström, M. Stalhammar, J. C. Budich, and E. J. Bergholtz, *Phys. Rev. B* **99**, 161115(R) (2019).
[18] Z.-S. Yang and J.-P. Hu, *Phys. Rev. B* **99**, 081102(R) (2019).

- [19] K. Kawabata, T. Bessho, and M. Sato, *Phys. Rev. Lett.* **123**, 066405 (2019).
- [20] M. S. Rudner and L. S. Levitov, *Phys. Rev. Lett.* **102**, 065703 (2009).
- [21] K. Esaki, M. Sato, K. Hasebe, and M. Kohmoto, *Phys. Rev. B* **84**, 205128 (2011).
- [22] S. Malzard, C. Poli, and H. Schomerus, *Phys. Rev. Lett.* **115**, 200402 (2015).
- [23] T. E. Lee, *Phys. Rev. Lett.* **116**, 133903 (2016).
- [24] D. Leykam, K. Y. Bliokh, C.-L. Huang, Y.-D. Chong, and F. Nori, *Phys. Rev. Lett.* **118**, 040401 (2017).
- [25] F. K. Kunst, E. Edvardsson, J. C. Budich, and E. J. Bergholtz, *Phys. Rev. Lett.* **121**, 026808 (2018).
- [26] Y. Xiong, *J. Phys. Commun.* **2**, 035043 (2018).
- [27] S.-Y. Yao and Z. Wang, *Phys. Rev. Lett.* **121**, 086803 (2018).
- [28] S.-Y. Yao, F. Song, and Z. Wang, *Phys. Rev. Lett.* **121**, 136802 (2018).
- [29] C.-H. Yin, H. Jiang, L.-H. Li, R. Lü, and S. Chen, *Phys. Rev. A* **97**, 052115 (2018).
- [30] Z.-P. Gong, Y. Ashida, K. Kawabata, K. Takasan, S. Higashikawa, and M. Ueda, *Phys. Rev. X* **8**, 031079 (2018).
- [31] K. Yokomizo and S. Murakami, *Phys. Rev. Lett.* **123**, 066404 (2019).
- [32] F. Song, S.-Y. Yao, and Z. Wang, *Phys. Rev. Lett.* **123**, 246801 (2019).
- [33] K.-I. Imura and Y. Takane, *Phys. Rev. B* **100**, 165430 (2019).
- [34] E. Edvardsson, F. K. Kunst, and E. J. Bergholtz, *Phys. Rev. B* **99**, 081302(R) (2019).
- [35] A. Mosfafaazadeh, *J. Math. Phys.* **43**, 205 (2002).
- [36] W.-J. Chen, Ş. K. Özdemir, G.-M. Zhao, J. Wiersig, and L. Yang, *Nature (London)* **548**, 192 (2017).
- [37] Y.-H. Lai, Y.-K. Lu, M.-G. Suh, Z.-Q. Yuan, and K. Vahala, *Nature (London)* **576**, 65 (2019).
- [38] M.-Z. Zhang, W. Sweeney, C. W. Hsu, L. Yang, A. D. Stone, and L. Jiang, *Phys. Rev. Lett.* **123**, 180501 (2019).
- [39] Y. Choi, C. Hahn, J. W. Yoon, S. H. Song, and P. Berini, *Nat. Commun.* **8**, 14154 (2017).
- [40] J. W. Yoon, Y. Choi, C. Hahn, G. Kim, S. H. Song, K.-Y. Yang, J. Y. Lee, Y. Kim, C. S. Lee, J. K. Shin, H.-S. Lee, and P. Berini, *Nature (London)* **562**, 86 (2018).
- [41] M.-A. Miri and A. Alù, *Science* **363**, eaar7709 (2019).
- [42] O. Latinne, N. J. Kylstra, M. Dörr, J. Purvis, M. Terao-Dunseath, C. J. Joachain, P. G. Burke, and C. J. Noble, *Phys. Rev. Lett.* **74**, 46 (1995).
- [43] R. Lefebvre, O. Atabek, M. Šindelka, and N. Moiseyev, *Phys. Rev. Lett.* **103**, 123003 (2009).
- [44] R. Uzdin, A. Mailybaev, and N. Moiseyev, *J. Phys. A* **44**, 435302 (2011).
- [45] M. V. Berry and R. Uzdin, *J. Phys. A* **44**, 435303 (2011).
- [46] T. J. Milburn, J. Doppler, C. A. Holmes, S. Portolan, S. Rotter, and P. Rabl, *Phys. Rev. A* **92**, 052124 (2015).
- [47] Ş. K. Özdemir, S. Rotter, F. Nori, and L. Yang, *Nat. Mater.* **18**, 783 (2019).
- [48] J. Doppler, A. A. Mailybaev, J. Böhm, U. Kuhl, A. Girschik, F. Libisch, T. J. Milburn, P. Rabl, N. Moiseyev, and S. Rotter, *Nature (London)* **537**, 76 (2016).
- [49] X.-L. Zhang, S.-B. Wang, B. Hou, and C. T. Chan, *Phys. Rev. X* **8**, 021066 (2018).
- [50] Q.-H. Song, M. Odeh, J. Zúñiga-Pérez, B. Kanté, and P. Genevet, *Science* **373**, 1133 (2021).
- [51] W.-J. Chen, M. Abbasi, Yogesh N. Joglekar, and K. W. Murch, *Phys. Rev. Lett.* **127**, 140504 (2021).
- [52] W.-J. Chen, M. Abbasi, B. Ha, S. Erdamar, Y. N. Joglekar, and K. W. Murch, *Phys. Rev. Lett.* **128**, 110402 (2022).
- [53] L.-Y. Ding, K.-Y. Shi, Y.-X. Wang, Q.-X. Zhang, C.-H. Zhu, L.-D. Zhang, J.-Q. Yi, S.-N. Zhang, X. Zhang, and W. Zhang, *Phys. Rev. A* **105**, L010204 (2022).
- [54] W.-Q. Liu, Y. Wu, C.-K. Duan, X. Rong, and J.-F. Du, *Phys. Rev. Lett.* **126**, 170506 (2021).
- [55] Z.-J. Ren, D. Liu, E.-T. Zhao, C.-D. He, K. K. Pak, J. Li, and G.-B. Jo, *Nat. Phys.* **18**, 385 (2022).
- [56] J. Dalibard, Y. Castin, and K. Mølmer, *Phys. Rev. Lett.* **68**, 580 (1992).
- [57] H. J. Carmichael, *Phys. Rev. Lett.* **70**, 2273 (1993).
- [58] F. Minganti, A. Miranowicz, R. W. Chhajlany, I. I. Arkhipov, and F. Nori, *Phys. Rev. A* **101**, 062112 (2020).
- [59] P. Kumar, K. Snizhko, and Y. Gefen, *Phys. Rev. A* **104**, L050405 (2021).
- [60] J. Li, A. K. Harter, J. Liu, L. de Melo, Y. N. Joglekar, and L. Luo, *Nat. Commun.* **10**, 855 (2019).
- [61] F. Minganti, A. Miranowicz, R. W. Chhajlany, and F. Nori, *Phys. Rev. A* **100**, 062131 (2019).